Analysis of a MEMS Transmission Line

Ari T. Alastalo, Tomi Mattila, *Member, IEEE*, and Heikki Seppä

***Abstract*—A microelectromechanical system (MEMS) sound waveguide is considered as a transmission line for RF signals. We analyze a device geometry of a straight one-dimensional microsize silicon rod, where a longitudinal acoustic wave is generated and detected using capacitive transducers. Linear, isotropic, and nondispersive acoustic-wave propagation is assumed. Based on the calculation of the electromechanical impedance, an electrical equivalent model is derived for the acoustic transmission line. A numerical example and a comparison to measured properties of a MEMS–transmission-line resonator shows that the characteristic impedance level of the waveguide is typically high, which causes challenges for matched termination. Solutions to overcome the matching problems are discussed.**

***Index Terms*—Electromechanical coupling, microelectromechanical system (MEMS) devices, RF MEMS, transmission line, waveguide.**

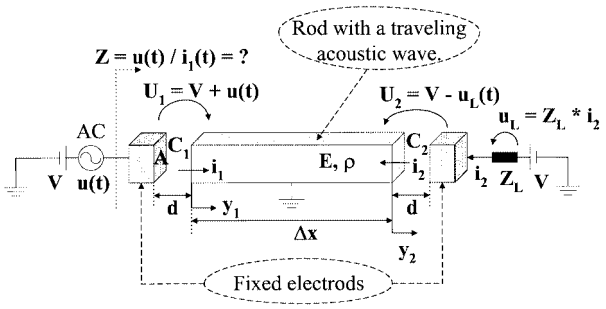

Fig. 1. Schematic representation of a setup where an electric signal is transmitted through a micromechanical rod as an acoustic plane longitudinal wave. Coupling between the electric signal and acoustic wave is done capacitively at both ends of the rod.

I. Introduction

ACOUSTIC-WAVE propagation in solids is an old and widely studied topic [1], [2]. Typical applications, such as delay lines, filters, and resonators, bear an analogy with the microwave electromagnetic devices [1], [3]. Acoustic wave theory is extensively used e.g. in bulk acoustic-wave (BAW) resonators and surface acoustic-wave (SAW) filters [3], [4]. The recent advances in microelectromechanical system (MEMS) technology have opened the possibility for creating miniaturized acoustical devices. As an example, a micromechanical resonator based on BAW operation has been demonstrated to be well suited for creating a high spectral purity oscillator [5]. Integrability with CMOS electronics, as well as size reduction and power savings of MEMS components compared to off-chip solutions (such as SAW devices) facilitate design of efficient single-chip radio transceivers that could revolutionize wireless communication devices [6]–[8].

In this paper, we investigate the possibility of creating microacoustical components, such as delay lines, for RF signals. We focus on a typical device geometry of a straight one-dimensional microsize silicon rod, where a longitudinal acoustic wave is generated and detected using capacitive transducers. Linear, isotropic, and nondispersive acoustic-wave propagation is assumed.[1] Based on the calculation of the electromechanical impedance, an electrical equivalent model is derived for the acoustic transmission line. The acoustic reflection and voltage transmission at the receiving transducer are evaluated using typical values for electrostatic coupling. The results show that obtaining perfect nonreflecting termination for the microsize transmission line is not straightforward, but requires tailored impedance-transforming techniques.

Manuscript received December 19, 2002; revised February 27, 2003.

The authors are with VTT Information Technology, Microsensing, Espoo FIN-02044 VTT, Finland (e-mail: ari.alastalo@vtt.fi).

Digital Object Identifier 10.1109/TMTT.2003.815270

[1]For a review of nonlinear and dispersive one-dimensional models see, e.g., [9] and the references therein.

II. Electromechanical Modeling

The setup that we are considering is schematically illustrated in Fig. 1. An electric signal is capacitively coupled to and from the MEMS rod at both ends through fixed electrodes. The rod is allowed to vibrate longitudinally between the electrodes to enable wave propagation along the rod. The rod is assumed to be anchored to the surrounding structures such that the wave propagation is not notably disturbed. In practice, the circuitry to connect the bias and signal voltages, as well as the shape of the electrodes and other details can differ from the simplified system of Fig. 1, which, however, captures the relevant physical properties. Some generalizations, e.g., for nonsymmetric bias, will be discussed after analyzing the system of Fig. 1. The electrodes and waveguide can be fabricated, e.g., on a device layer of a silicon-on-insulator (SOI) wafer. To reduce dissipation caused by air friction to moving MEMS structures, the device can be packaged in a vacuum.

In Fig. 1, V is a constant bias voltage applied to the electrodes at both ends of the rod and $u(t)$ is a time-dependent signal voltage at the left (input) electrode. The signal is taken to be harmonic $u(t) = u_0 \exp(j\omega t)$. The signal voltage $u(t)$ induces currents $i_1(t)$ and $i_2(t)$ through the input (left-hand side) and output (right-hand side) transducer capacitors C_1 and C_2, respectively. Consequently, voltage across the load impedance Z_L is $u_L(t) = Z_L i_2(t)$. Since the rod is grounded, voltages $U_1(t) = V + u(t)$ and $U_2(t) = V - u_L(t)$ are seen across the transducer capacitors. The rod has a length Δx, a constant

cross-sectional area A, Young's modulus E, density ρ, and is assumed to have no mechanical[2] or electrical[3] losses. When no voltages are applied ($U_1 = U_2 = 0$), the gap between the rod and electrodes is d at both ends. With nonzero voltages, the ends of the rod are displaced by y_1 and y_2, as shown in Fig. 1. We assume the transducer capacitors to be ideal parallel-plate capacitors with capacitances $C_1 = \epsilon_0 A/(d + y_1)$ and $C_2 = \epsilon_0 A/(d - y_2)$. The voltages across and currents through the capacitors are thus related by $i_1 = d(C_1 U_1)/dt$ and $i_2 = d(C_2 U_2)/dt$. We further assume that the voltage sources are ideal with no internal losses. The electric input impedance is now $Z = u(t)/i_1(t)$.

We assume that the voltages $u(t)$ and $u_L(t)$ are small with respect to the bias voltage V and that the displacements y_1 and y_2 are much smaller than the zero-voltage gap d. We also assume the system to be linear. Expanding the currents i_1 and i_2 up to linear order in the small parameters (u/V), (u_L/V), (y_1/d), and (y_2/d), we obtain

$$i_1 = j\omega C_0 u - \eta \dot{y}_1 \tag{1a}$$

$$i_2 = \frac{\eta \dot{y}_2}{1 + j\omega C_0 Z_L}. \tag{1b}$$

Here, $C_0 \equiv \epsilon_0 A/d$ is the zero-voltage capacitance and $\eta \equiv C_0 V/d$ is the electromechanical coupling constant. For vanishing mechanical motion, the electric input impedance is from (1a) $Z = Z_0 \equiv 1/(j\omega C_0)$.

For the forces f_1 and f_2 exerted by the capacitors C_1 and C_2 to the left- and right-hand-side ends of the rod, respectively, one finds through $f = (1/2)U^2 dC/dy$ up to linear order

$$f_1 = \eta\left(\frac{V}{2} + u\right) - k_e y_1 \tag{2a}$$

$$f_2 = \frac{\eta V}{2} + k_e y_2 - \gamma \dot{y}_2 \tag{2b}$$

where $k_e \equiv V\eta/d$ is the electrical spring-softening term and $\gamma \equiv \eta^2 (Z_L || Z_0)$ (Z_L and Z_0 in parallel) is a complex damping coefficient. Here, the sign of f_1 is selected as shown in Fig. 2. k_e usually represents only a small correction and can be omitted.

The mechanical model is now as follows. The longitudinal displacement field $y(x,t)$ of the rod obeys a wave equation

$$\frac{\partial^2 y(x,t)}{\partial t^2} = c^2 \frac{\partial^2 y(x,t)}{\partial x^2}, \qquad t \geq 0; \quad x \in [0, \Delta x] \tag{3}$$

with boundary conditions following from (2a) and (2b) assuming Hooke's law to be valid:

$$\left.\frac{\partial y(x,t)}{\partial x}\right|_{x=0} = \frac{f_1}{AE} \qquad \left.\frac{\partial y(x,t)}{\partial x}\right|_{x=\Delta x} = \frac{f_2}{AE} \tag{4}$$

and has a harmonic time dependence due to the harmonic force. Here, $c \equiv \sqrt{E/\rho}$ is the phase velocity of the longitudinal wave. The mechanical model is illustrated in Fig. 2.

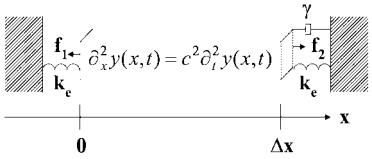

Fig. 2. Mechanical equivalent model of the setup of Fig. 1. Here, $\partial_x^2 y$ and $\partial_t^2 y$ are shorthand notations for the second-order space and time derivatives of the displacement field, respectively.

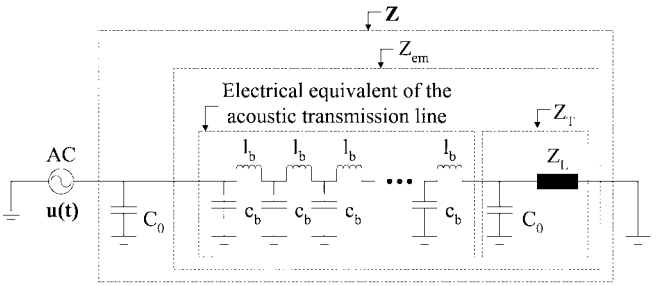

Fig. 3. Electrical small-signal equivalent model of Fig. 1.

III. Analytical Solution

A solution to the wave-propagation problem of (3) and (4) is found by subtracting a time-independent zero-signal solution $y_0(x)$ from the displacement field $y(x,t)$ and seeking a solution in the form

$$\bar{y}(x,t) = \left(Be^{((j\omega x)/c)} + De^{((-j\omega x)/c)}\right) e^{j\omega t} \tag{5}$$

for the deviation $\bar{y}(x,t) \equiv y(x,t) - y_0(x)$, which also satisfies the wave equation (3) and a zero-bias form of the boundary conditions (4). For the current i_1 in (1a) through the input capacitor C_1, we find

$$i_1(t) = j\omega C_0 u(t) - \eta \dot{\bar{y}}(0,t) = \frac{u(t)}{Z} \equiv u(t)\left(\frac{1}{Z_0} + \frac{1}{Z_{\rm em}}\right) \tag{6}$$

where the electromechanical impedance (see Fig. 3)

$$Z_{\rm em} \equiv \frac{j u_0}{\eta\omega(B + D)} \tag{7}$$

[2]We assume that despite doping and imperfections, acoustic properties of the SOI device layer material can be approximated by those of single-crystal silicon within the frequency range of interest. At $f = 10$ MHz, for longitudinal plane-wave propagation in cube-edge direction in single-crystal bulk silicon, one has an attenuation factor of $\alpha \approx 10^{-4}$ dB/mm $\propto f^2$ [1]. This corresponds to an acoustical quality factor of $Q \approx 3.3 \times 10^5 \propto 1/f$ [1]. An electrical equivalent resistance R_s, of the mechanical dissipation over a distance of 1 mm, in series with a load resistance R_L is found by voltage division to be $R_s = R_L(10^{\alpha \times 1\ \rm mm/20} - 1)$. For $\alpha = 10^{-4}$ dB/mm at $f = 10$ MHz, we find $R_s = R_L \times 10^{-5}$. For longitudinal wave propagation in a micromechanical narrow rod, a quality factor of $Q \approx 1.8 \times 10^5$ has been reported [5], which is only half of the bulk value above and yields a doubling of α and R_s. Thus, at least for frequencies in the range of 10 MHz, mechanical losses can be neglected for small systems.

[3]In practice, one places electrical ground connections closer to the ends of the rod and not only in the middle, as shown in Fig. 1, for simplicity. This is in order to reduce dissipation caused by nonzero resistivity r_b of the rod material. Groundings can be done in places where the rod is hanged to the surrounding structures. Details of hanging are not studied in this paper. Resistance at the ends of the rod can be calculated as $R_b = r_b l_g/A$, where l_g is the distance from the end of the rod to the closest grounding and A is the cross-sectional area of the rod. For the heavily boron-doped material of [5] ($r_b \approx 2 \times 10^{-4}$ Ωm [14]), with $l_b = 100\,\mu$m and $A = 100\,\mu\text{m} \times 10\,\mu$m, one finds $R_b \approx 20\ \Omega$, which, as will be seen, is much smaller than other typical impedances of the system and will be ignored in this paper. If taken into account, R_b becomes in series with the capacitances C_0 in Fig. 3.

expresses the coupling of the electric signal to the mechanical motion and is, thus, the quantity of primary interest here. Substituting (5) to the boundary conditions (4) with zero bias allows one to solve for the unknown coefficients B and D and to obtain $Z_{\rm em}$ in (7). For simplicity, we only consider the case where $k_e = 0$, which generally is a good approximation for practical MEMS structures. Consequently, one obtains the standard expression [2], [10], [11]

$$Z_{\rm em} = Z_b \frac{Z_T + Z_b \tanh(j\beta\Delta x)}{Z_b + Z_T \tanh(j\beta\Delta x)} \tag{8}$$

where $\beta \equiv \omega/c$, $Z_b \equiv AE/(c\eta^2)$, and $Z_T \equiv Z_0 || Z_L$ (see Fig. 3). The mechanical losses can be included in (8) by substituting $j\beta$ with $j\beta + \alpha$, where α is the attenuation coefficient [1], [10], [11].

The mechanical amplitude reflection coefficient for the right-hand-side end of the rod can be expressed as

$$r^2 \equiv \left|\frac{B}{D}\right|^2 = \left|\frac{Z_T - Z_b}{Z_T + Z_b}\right|^2. \tag{9}$$

For zero reflection, one needs $Z_T = Z_b$, which gives with (8)

$$Z_{\rm em} = Z_b = \frac{AE}{c\eta^2} = \frac{A\sqrt{\rho E}}{\eta^2} = \frac{d^4\sqrt{\rho E}}{A(\epsilon_0 V)^2} \equiv R_{\rm em}. \tag{10}$$

Here, $Z_c \equiv A\sqrt{\rho E}$ is the mechanical characteristic impedance of the rod [2]. The corresponding matched load impedance is $Z_L = (R_{\rm em} || Z_0^*)$. The above discussion shows that $Z_b = Z_c/\eta^2$ can be seen as an electrical characteristic impedance of the acoustic waveguide. One can thus relate the inductance l_b and capacitance c_b densities in Fig. 3 to Z_b and to the phase velocity c through $Z_b = \sqrt{l_b/c_b}$ and $c = 1/\sqrt{l_b c_b}$. One finds $l_b = A\rho/\eta^2$, and $c_b = \eta^2/(AE)$ that are similar to the corresponding relations known for MEMS resonators [5].

Of interest are also the current i_2 in (1b) through the output capacitor and the voltage $u_L = Z_L i_2$ across the load impedance. The transfer impedance $Z_{12} \equiv u(t)/i_2(t)$ is found similarly to the input-impedance calculation above as follows:

$$Z_{12} = \frac{-ju_0\left(1 + \dfrac{Z_L}{Z_0}\right)}{\omega\eta\left(Be^{((j\omega\Delta x)/c)} + De^{-((j\omega\Delta x)/c)}\right)} \tag{11}$$

and gives the load voltage through $u_L = i_2 Z_L = u\, Z_L/Z_{12}$. In particular, for the matched load, one finds

$$u_L = u\big(-\cos(\beta\Delta x) + j\sin(\beta\Delta x)\big) = -ue^{-((j\omega\Delta x)/c)} \tag{12}$$

in which case, the acoustic waveguide only introduces a sign change and a phase shift to the electric signal and delivers a power of $|u|^2/(2Z_b)$ to the load.

If the matched load is represented by an inductance[4] of $L_{\rm em} \equiv 1/(\omega_0^2 C_0)$ in parallel with a resistance of $R_{\rm em}$, transmission through the line becomes bandpass centered at ω_0 with a 3-dB bandwidth of $W_{\rm 3dB} \equiv 1/(2\pi R_{\rm em} C_0)$. Due to the reactances in the system, it is now possible that the load voltage u_L exceeds the source voltage u. This can be prevented by requiring $\cos(\omega_0\Delta x/c) = 0 \Rightarrow \Delta x = \lambda/4 + n\lambda/2 (n \in \{0, 1, 2, \ldots\})$.

[4]Wide-band termination would require a reactance of $+j/(\omega C_0)$.

IV. Generalization of the System

More insight is gained by separating the problem into electrical and mechanical propagation. This is conveniently done by introducing transmission matrices. We take the mechanical equivalent of voltage u and current i to be negative of the force field $(-f)$ and the velocity field (v) in the waveguide. The mechanical impedance along the waveguide is now $Z_m \equiv -f/v$. The input (left-hand side) end current and force relations (1a) and (2a) now give

$$\begin{pmatrix} u \\ i_1 \end{pmatrix} = -\frac{1}{\eta_1}\begin{pmatrix} 1 & 0 \\ j\omega C_{0,1} & \eta_1^2 \end{pmatrix}\begin{pmatrix} -f_1 \\ v_1 \end{pmatrix} \equiv T_{\rm in}\begin{pmatrix} -f_1 \\ v_1 \end{pmatrix} \tag{13}$$

where $T_{\rm in}$ is the left-hand-side-end transmission matrix. Here, η_1 and $C_{0,1}$ denote η and C_0 at the input end. Similarly for the right-hand-side (output) end, one finds from (1b) and (2b)

$$\begin{pmatrix} -f_2 \\ v_2 \end{pmatrix} = -\frac{1}{\eta_2}\begin{pmatrix} \eta_2^2 & 0 \\ j\omega C_{0,2} & 1 \end{pmatrix}\begin{pmatrix} u_L \\ i_2 \end{pmatrix} \equiv T_{\rm out}\begin{pmatrix} u_L \\ i_2 \end{pmatrix} \tag{14}$$

with η_2 and $C_{0,2}$ denoting η and C_0 at the right-hand-side transducer. The mechanical propagation is given by the familiar waveguide transmission matrix

$$\begin{aligned}\begin{pmatrix} -f_1 \\ v_1 \end{pmatrix} &= \begin{pmatrix} \cos(\beta\Delta x) & jZ_c\sin(\beta\Delta x) \\ j\sin\dfrac{(\beta\Delta x)}{Z_c} & \cos(\beta\Delta x) \end{pmatrix}\begin{pmatrix} -f_2 \\ v_2 \end{pmatrix} \\ &\equiv T_{\rm mech} \times (-f_2, v_2)^T \end{aligned} \tag{15}$$

yielding for mechanical impedances the same result shown above in (8) for the electromechanical impedance (with interchanges $Z_{\rm em} \leftrightarrow Z_1$, $Z_T \leftrightarrow Z_2$, and $Z_b \leftrightarrow Z_c$). The electrical input impedance Z is now found using the total transmission matrix of the system $T_{\rm tot} \equiv T_{\rm in} T_{\rm mech} T_{\rm out}$ from $(u, i_1)^T = T_{\rm tot} \times (u_L, i_2)^T$.

The matrix formulation enables one to consider more general situations with, for example, nonsymmetric bias or transducer geometries. Also, other transducer coupling mechanisms can be considered. The formulation also applies to different waveguide geometries, e.g., with varying cross-sectional area, for which the transmission matrix can be formulated. Furthermore, anchoring effects can be taken into account.

V. Numerical Example

Table I shows η, C_0, resistance $R_{\rm em}$, inductance $L_{\rm em}$, and bandwidth $W_{\rm 3dB}$ at center frequency $f_0 = 10.573$ MHz for a 1-mm-long silicon rod ($E = 166.7$ GPa, $\rho = 2330\ {\rm kg/m^3} \Rightarrow c \approx 8458$ m/s [5]) with $A = 8\ \mu{\rm m} \times 10\ \mu{\rm m}$ and $A = 8\ \mu{\rm m} \times 100\ \mu{\rm m}$ (one of the dimensions is limited by the typical height of the device layer of the SOI wafer), and $V = 100$ V. The center frequency is selected to obey $\cos(\omega_0\Delta x/c) = 0$ (see discussion in Section III). We consider three different values for the gap d (reaching a controllable gap size of 0.1 μm has been demonstrated [12]). The values of Table I (such as $R_{\rm em} = 3\ M\Omega$ for $d = 0.1\ \mu m$ and $A = 8\ \mu{\rm m} \times 100\ \mu{\rm m}$) reveal that, for practical realization of the MEMS waveguide, impedance matching is a challenge. This is because the weakness of the capacitive coupling makes the characteristic electrical impedance of the waveguide extremely high.

TABLE I
PARAMETERS FOR MATCHED TERMINATION OF AN ACOUSTIC TRANSMISSION LINE AT $f = 10.573$ MHz

A \ d	1 μm	0.5μm	0.1μm	variable
8 × 10	0.07	0.28	7.1	η / [μFV/m]
8 × 100	0.7	2.8	71	
8 × 10	0.7	1.4	7.1	C_0 / [fF]
8 × 100	7	14	71	
8 × 10	310	20	0.030	$R_{\rm em}$ / [GΩ]
8 × 100	31	2	0.003	
8 × 10	320	160	32	$L_{\rm em}$ / [mH]
8 × 100	32	16	3.2	
8 × 10	0.72	5.7	720	$W_{\rm 3dB}$ / [kHz]
8 × 100	0.72	5.7	720	
μ m × μ m				

Equation (10) shows that $R_{\rm em}$ can be made smaller by having a smaller gap d, softer or sparser rod material (smaller E or ρ), a larger area A, higher permittivity material in the gap, or a higher bias voltage V. On the other hand, the maximum displacement of the end of the rod is limited by $y_{\max} < \xi d$, where $\xi \approx 0.3$, in order to avoid pull-in. Considering only the bias voltage V, it is easy to show that the requirement to avoid pull-in leads to a lower limit for $R_{\rm em}$ as follows:

$$R_{\rm em} > R_{\rm em}^{\rm min} \equiv \frac{\sqrt{\rho}}{AE^{(5/6)}} \left(\frac{V}{\epsilon_0}\right)^{(2/3)} \left(\frac{\Delta x}{0.6}\right)^{(4/3)}. \quad (16)$$

For example, in Table I, with $R_{\rm em} = 3$ MΩ, we have $R_{\rm em}^{\rm min} \approx 2.7$ MΩ for a 1-mm-long rod. Increasing now the bias voltage by a factor of ten, decreases $R_{\rm em}$ to 30 kΩ, but leads to $R_{\rm em}^{\rm min} > R_{\rm em}$, resulting in pull-in. Thus, both (10) and (16) must be taken into account. One candidate for a softer and sparser rod material is porous silicon. For example, for a porosity of 60%, the Young's modulus is reported to drop almost 90% of the value for nonporous material [13]. This would divide $R_{\rm em}$ by five, but also yield a four times larger $R_{\rm em}^{\rm min}$.

Fig. 4 shows the voltage ratio u_L/u and mechanical reflection coefficient r^2 when an inductor of $L_{\rm em} = 1/(\omega_0^2 C_0)$ is used to tune out the transducer capacitance. The solid curves are for a center frequency satisfying $\cos(\omega_0 \Delta x/c) = 0$, while, for the dashed curves, a slightly different frequency with $\cos(\omega_0 \Delta x/c) \neq 0$ is considered.

VI. COMPARISON TO EXPERIMENTS

The characteristic impedance of the MEMS transmission line can feasibly be probed in the short- or open-circuited resonator configuration [10], [11], when the quality factor Q of the resonator is sufficiently large. For example, for an open-circuited transmission-line resonator, the lumped-element values for an equivalent *RLC* series-resonant circuit are $R = r_b \Delta x/2$, $L = \pi Z_b/(4\omega_0)$, and $C = 1/(L\omega_0^2)$ [11]. Here, $\Delta x = \lambda_0/4$ is the length of the line, λ_0 is the wavelength corresponding to the resonant frequency ω_0, Z_b is the electrical characteristic impedance of the waveguide in (10), and r_b is the resistance per unit length of the line. The equivalent *RLC* circuit is valid in the vicinity of the resonant frequency. Since losses in the waveguide are not considered in this paper, resistance r_b is not shown in Fig. 3 in series with the inductance l_b. Measurements for such a high-Q MEMS transmission-line resonator were reported in [5] at 11.75 MHz corresponding to $\Delta x = 180\,\mu$m. Other resonator dimensions and parameter values of [5] were the same as here in Table I with $d = 1\,\mu$m and $A = 8\,\mu\text{m} \times 10\,\mu$m. The parameter values for the equivalent *RLC* circuit were obtained through fitting the simulation results to the measured data. In particular, it was found in [5] that $C = 0.05$ aF and $L = 3.62$ kH. Using the results of this paper, one obtains $L = \pi Z_b/(4\omega_0) = 3.34$ kH and $C = 1/(L\omega_0^2) = 0.05$ aF, which are in good agreement with the measurement-based values of [5]. Direct experimental study of the transmission-line operation of the MEMS waveguide requires solution to the impedance-matching problem that is one of the focuses of future research in this area.

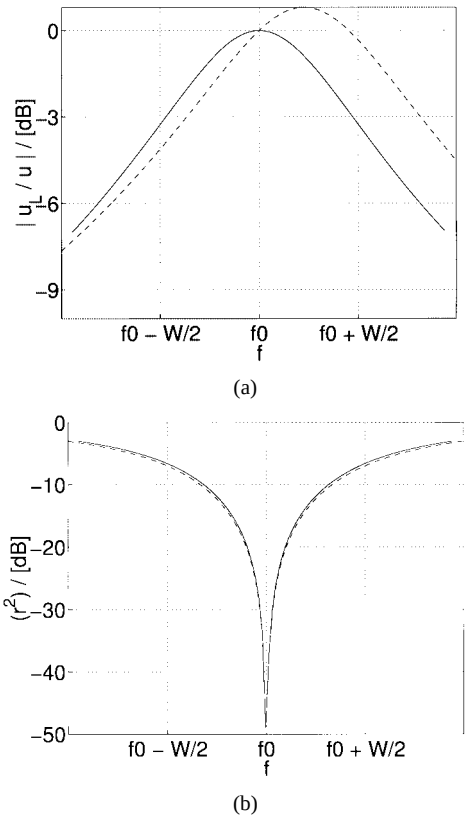

Fig. 4. (a) Voltage transmission $|u_L/u|$ and (b) mechanical reflection coefficient r^2 for center frequencies $f_0 = 10.573$ MHz (solid line) and $f_0 = 10$ MHz (dashed line). Other parameter values are the same as in Table I with the larger values of area and gap.

VII. DISCUSSION AND CONCLUSIONS

Using sound waveguides as delay lines for RF signals is desirable since much smaller group velocities can be reached than with electromagnetic waveguides. However, impedance levels needed for efficient signal transmission through an acoustic waveguide become extremely high, as shown in this paper, for a single-crystal silicon rod with capacitive coupling. This is due to the weakness of the electromechanical coupling constant. Thus, one needs to consider different coupling mechanisms, softer and sparser rod materials, electrical and mechanical impedance transformations, and other structures for acoustic-wave propagation. It is easy to show that, for example, with a microsize piezoelectric quartz transducer,

one does not reach a stronger coupling to a silicon rod when the length of the rod is much larger than the transducer size and when small enough capacitor gaps (of the order of half a micrometer) and high enough bias voltages (tens of volts) can be used. On the other hand, high-Q values of microelectromechanical resonators suggest that, at least for narrow bandwidths below 100 MHz, mechanical impedance transformation can enable efficient acoustic waveguide operation with capacitive coupling.

REFERENCES

[1] B. A. Auld, *Acoustic Fields and Waves in Solids*, 2nd ed. Melbourne, FL: Krieger, 1990, vol. 1.

[2] H. F. Pollard, *Sound Waves in Solids*. London, U.K.: Pion Ltd., 1977.

[3] J. F. Rosenbaum, *Bulk Acoustic Wave Theory and Devices*. Boston, MA: Artech House, 1988.

[4] D. P. Morgan, *Surface-Wave Devices for Signal Processing*. Amsterdam, The Netherlands: Elsevier, 1991.

[5] T. Mattila, J. Kiihamäki, T. Lamminmäki, O. Jaakkola, P. Rantakari, A. Oja, H. Seppä, H. Kattelus, and I. Tittonen, "A 12 MHz bulk acoustic micromechanical oscillator," *Sens. Actuators A, Phys.*, vol. 101, pp. 1–9, Sept. 2002.

[6] C. T.-C. Nguyen, "Frequency-selective MEMS for miniaturized low-power communication devices," *IEEE Trans. Microwave Theory Tech.*, vol. 47, pp. 1486–1503, Aug. 1999.

[7] D. F. Moore and R. R. A. Syms, "Recent developments in micromachined silicon," *Electron. Commun. Eng. J.*, vol. 11, no. 6, pp. 261–270, Dec. 1999.

[8] J. J. Yao, "RF MEMS from a device perspective," *J. Micromech. Microeng.*, vol. 10, pp. R9–R38, 2000.

[9] V. I. Erofeev and N. V. Klyueva, "Solitons and nonlinear periodic strain waves in rods, plates, and shells (a review)," *Acous. Phys.*, vol. 48, no. 6, pp. 643–655, 2002.

[10] D. M. Pozar, *Microwave Engineering*, 2nd ed. New York: Wiley, 1998.

[11] R. E. Collin, *Foundations for Microwave Engineering*. New York: McGraw-Hill, 1966.

[12] W.-T. Hsu, J. R. Clark, and C. T.-C. Nguyen, "A sub-micron capacitive gap process for multiple-metal-electrode lateral micromechanical resonators," in *Proc. IEEE MEMS Conf.*, Interlaken, Switzerland, 2001, pp. 349–352.

[13] D. Bellet, P. Lamagnère, A. Vincent, and Y. Brèchet, "Nanoindentation investigation of the Young's modulus of porous silicon," *J. Appl. Phys.*, vol. 80, no. 7, pp. 3772–3776, Oct. 1996.

[14] S. M. Sze, *Semiconductor Devices*, 2nd ed. New York: Wiley, 2002.

Ari T. Alastalo received the M.Sc. degree in technical physics from Helsinki University of Technology (HUT), Helsinki, Finland, in 1997.

From 1996 to 1998, he was an Assistant with HUT, where he was involved in the area of magnetic quantum impurities. From 1998 to 2001, he was with the Nokia Research Center, where he carried out research on radio propagation, RF architectures, baseband algorithms, and protocols for adaptive-antenna systems. Since 2002, he has been a Research Scientist with VTT Information Technology, Espoo, Finland. His current research focuses on RF MEMS.

Tomi Mattila (M'01) received the M.Sc. and Dr.Tech. degrees in technical physics from the Helsinki University of Technology (HUT), Helsinki, Finland, in 1994 and 1997, respectively.

From 1997 to 1999, he was a Post-Doctoral Research Fellow with National Renewable Energy Laboratory, Golden, CO. Since 1999, he has been a Senior Research Scientist with VTT Information Technology, Espoo, Finland. His current research interests concentrate on micromechanical RF devices.

Heikki Seppä received the M.Sc., Lic. Tech., and Dr. Tech. degrees in technology from the Helsinki University of Technology (HUT), Helsinki, Finland, in 1977, 1979 and 1989, respectively.

From 1976 to 1979, he was an Assistant with HUT, where he was involved in the area of electrical metrology. In 1979, he joined the Technical Research Centre of Finland (VTT), Espoo, Finland, where, since 1989, he has been a Research Professor. In 1994, he became Head of the measurement technology field with VTT, and in 1996–1998, he was Research Director of VTT automation. Since 2002, he has been the Research Director of VTT Information Technology. He has performed research, in general, on electrical metrology and, in particular, on superconducting devices for measurement applications. He also conducts research on dc superconducting quantum interference devices (SQUIDs), quantized Hall effect, mesoscopic devices, RF instruments, and MEMS devices.